PAPER

NJC
www.rsc.org/njc

# Anion binding to azamacrocycles: synthesis and X-ray crystal structures of halide adducts of [12]aneN$_4$ and [18]aneN$_6$

**Andrew C. Warden,[a] Mark Warren,[a] Milton T. W. Hearn[b] and Leone Spiccia*[a]**

[a] *School of Chemistry, Monash University, Clayton, Victoria, Australia, 3800. E-mail: leone.spiccia@sci.monash.edu.au*

[b] *Centre for Green Chemistry, School of Chemistry, Monash University, Clayton, Victoria, Australia, 3800*

***Received (in Durham, UK) 6th February 2004, Accepted 26th May 2004***
***First published as an Advance Article on the web 21st July 2004***

An investigation into the halide binding properties of two polyazamacrocycles [12]aneN$_4$ (**L1**) and [18]aneN$_6$ (**L2**) has resulted in the determination of the molecular structure of five compounds [H$_4$**L1**(Br)$_4$]·2H$_2$O (**1**), [H$_2$**L1**(I$_3$)$_2$]·2I$_2$·2CH$_3$CN (**2**), [H$_6$**L2**(Cl)$_6$]·4H$_2$O (**3**), [H$_4$**L2**(Br)$_4$]·2H$_2$O (**4**) and [H$_4$**L2**(I)$_2$(I$_3$)$_2$] (**5**). [18]aneN$_6$ (**L2**) was generally found to bind two anions within the macrocyclic cavity. In the adducts formed by [12]aneN$_4$ (**1** and **2**), the anions and solvent of crystallization do not sit within the [12]aneN$_4$ cavity, instead preferring to occupy positions exterior to the macrocycle. Left- and right-handed helices are formed by the I$_3^-$ and I$_2$ moieties in **2** that house acetonitrile solvent molecules in the centre of the spiral. In most cases, chloride and bromide adopt trigonal pyramidal co-ordination motifs with various degrees of distortion from a regular geometry. The ring size, conformational flexibility and level of protonation were found to influence the halide binding characteristics of the macrocycles.



## Introduction

Although the complexation of metal ions and other cationic guests to organic ligands has been studied intensely, only recently has significant attention been directed upon the nature of anion binding to synthetic organic hosts (see ref. 1 and 2 for two recent reviews). With the rapid expansion of the protein and small molecules structural databases has come the opportunity to study in detail the various factors that contribute to anion transport and binding in biological and abiotic systems. Hosts containing NH and/or $NH_2^+$ moieties have been known as good binding agents for halides since Park and Simmons alluded to the key roles of electrostatic interactions and hydrogen bonding of katapinands in 1968,[3] which were subsequently structurally confirmed.[4] Since then a plethora of halide adducts, including those formed by azamacrocyclic cages,[5–9] porphyrins,[10–12] calix[*n*]pyrroles,[13–16] amide based compounds,[17–21] adenine,[22] imidazolium cyclophanes[23] and metal complexes,[24–26] have been structurally characterized, with particular attention being given to size complementarity in order to gain higher levels of selectivity and singular encapsulation of the desired anion. As a result of this focus, the halide binding properties of the monocyclic azamacrocycles have attracted comparatively little attention. One factor contributing to this is possibly their inherent lack of specificity. Constants for complex formation between [18]aneN$_6$ with the halides and other monoanions have been determined, most commonly using potentiometric and conductomeric titrations, and show variations of only 1–2 orders of magnitude.[31] A 1997 survey of the Cambridge Crystallographic Data Collection[27] showed that the most effective H-bond donor for halides is the [N–H]$^+$ functionality. This moiety promotes interactions with halides through a combination of electrostatic interactions and hydrogen bonding.[27] Computational analyses have also been used to study these associations[28–30] and a recent publication described the structures of several halide complexes of acyclic polyammonium hosts[32] with a view to examining the co-ordination behaviour of the halides in an unencumbered environment. In this vein, we have determined the structures of a series of halide complexes of the azamacrocycles, 1,4,7,10-tetraazacyclododecane (**L1**, [12]aneN$_4$) and 1,4,7,10,13,16-hexaazacyclooctadecane (**L2**, [18]aneN$_6$) *via* single crystal crystallographic studies. The macrocycles, while having some level of pre-organization, retain sufficient flexibility to enable them to adopt conformations and degrees of protonation that complement the binding preferences of the halides and to facilitate crystallization through the formation of H-bonded networks.

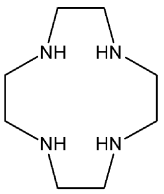


**L1**, [12]aneN$_4$

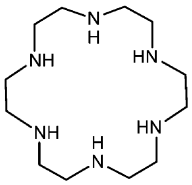


**L2**, [18]aneN$_6$

## Experimental section

### Materials and reagents

1,4,7,10-tetraazacyclododecane (**L1**, [12]aneN$_4$) was purchased from Strem Chemicals and used without further purification. All other reagents were obtained from commercial suppliers and used as supplied with the exception of 1,4,7,10,13,16-hexaazacyclooctadecane (**L2**, [18]aneN$_6$), which was isolated as reported previously.[33]

### Microanalyses and spectroscopy

Microanalyses were performed by the Campbell Microanalytical Service, University of Otago, New Zealand. Infrared spectra were recorded using KBr pellets on a Perkin-Elmer 1600 FTIR at a resolution of 8 cm$^{-1}$.

DOI: 10.1039/b401841a

## Synthesis

**$[H_4L1(Br)_4]\cdot 2H_2O$ (1). L1.** (125 mg, 0.72 mmol) was suspended in water (3.4 ml) and hydrobromic acid (conc., 1.20 g) was added. The solution was left to evaporate in the open atmosphere and, after several days, large, clear rhombohedral crystals had formed. Yield = 362 mg, 95%. Microanalysis (%) found: C 18.2; H 5.3; N 10.5. Calc'd for $C_8H_{28}N_4Br_4O_2$: C 18.1; H 5.3; N 10.5. Infrared spectrum ($\nu$, $cm^{-1}$): 3424 s, 3143 m, 2996 s, 2926 s, 2768 s, 2735 s, 1684 s, 2447 s, 1607 m, 1544 m, 1488 s, 1460 m, 1424 m, 1063 w, 1000 m, 963 w, 914 w, 758 m, 576 m.

**$[H_2L1(I_3)_2]\cdot 2I_2\cdot 2CH_3CN$ (2). L1.** (54 mg, 0.31 mmol) was suspended in water (2.5 ml) and hydriodic acid (conc., 600 mg) was added followed by ethanol (abs., 20 ml) and acetonitrile (10 ml). The solution was left to evaporate in the open atmosphere and produced very dark crystals of **2** after several days. Yield = 218 mg, 55%. Microanalysis (%) found: C 10.1; H 2.4; N 5.5. Calc'd for $C_{12}H_{28}N_6I_{10}$: C 9.5; H 1.9; N 5.5. Infrared spectrum ($\nu$, $cm^{-1}$): 3424 s, 3282 s, 3025 m, 2859 m, 1655 m, 1561 s, 1544 s, 1526 m, 1459 m, 1440 s, 1387 s, 1342 s, 1267 s, 1191 m, 1115 m, 1074 m, 1046 m, 1014 m, 958 w, 875 w, 812 s, 754 s, 522 m.

**$[H_6L2(Cl)_6]\cdot 4H_2O$ (3). L2.** (25 mg, 0.096 mmol) was dissolved in water (1 ml) and hydrochloric acid (conc., 1 ml) was added. The solution was left to evaporate in the open atmosphere and after several days produced clear crystals of **3**. Yield = 32 mg, 60%. Microanalysis (%) found: C 26.5; H 8.1; N 15.3. Calc'd for $C_{12}H_{44}N_6Cl_6O_4$: C 26.2; H 8.1; N 15.3. Infrared spectrum ($\nu$, $cm^{-1}$): 3379 s, 2998 s, 2681 s, 2440 s, 1653 m, 1607 m, 1564 w, 1544 w, 1500 m, 1481 m, 1444 s, 1409 m, 1366 w, 1325 w, 1283 w, 1103 w, 1052 m, 1008 m, 990 m, 947 m, 920 w, 873 w, 840 w, 792 m, 764 m, 556 m, 528 m.

**$[H_4L2(Br)_4]\cdot 2H_2O$ (4). L2.** (21 mg, 0.081 mmol) was dissolved in water (0.125 ml) and hydrobromic acid (conc., 1 ml) was added. The solution became cloudy and crystals deposited shortly afterwards. A further 4 ml of water was added and the solution heated to 70 °C to dissolve the microcrystalline mass. The solution was left open to the atmosphere and after several days produced large clear crystals. Microanalysis showed that the primary component was of composition $[H_6\mathbf{L2}Br_6]\cdot 2H_2O$, however, these crystals were unsuitable for X-ray diffraction studies. **4** was a minor component of the clear crystalline mass but due to intergrowth of the crystals separation was not achievable. Yield (total mass) = 44 mg, 89%. Microanalysis (%) found: C 17.9; H 5.2; N 11.8. Calc'd for $C_{12}H_{38}N_6Br_4O_2$ (**4**): C 23.3; H 6.2; N 13.6. Calc'd for $C_{12}H_{40}Br_6N_6O_2$ ($[H_6\mathbf{L2}Br_6]\cdot 2H_2O$): C 18.5; H 5.2; N 10.8. Infrared spectrum ($\nu$, $cm^{-1}$): 3409 s, 2965 s, 2763 s, 2504 s, 2455 s, 2373 s, 2342 m, 1637 w, 1603 m, 1556 w, 1530 w, 1496 m, 1473 m, 1441 s, 1364 w, 1323 w, 1282 w, 1099 m, 1047 m, 1002 m, 982 m, 937 m, 914 m, 865 m, 831 w, 783 m, 756 s, 551 w, 518 w.

**$[H_4L2(I)_2(I_3)_2]$ (5). L2.** (16 mg, 0.06 mmol) was dissolved in water (0.8 ml) and hydriodic acid (conc., 0.50 g) was added followed by ethanol (95%, 3 ml) and acetonitrile (3.7 ml). A small amount of a light yellow precipitate formed immediately. The dark solution was left to evaporate slowly in the open atmosphere and after several days produced very dark crystals of **5** which were separated from the yellow component. Yield = 26 mg, 68%. Microanalysis (%) found: C 9.1; H 2.1; N 5.4. Calc'd for $C_{12}H_{34}N_6I_{10}$ (**5** co-crystallized with one molecule of $I_2$): C 9.4; H 2.2; N 5.5. Infrared spectrum ($\nu$, $cm^{-1}$): 3449 m, 3276 w, 3004 s, 2847 m, 1544 w, 1510 w, 1440 m, 1411 m, 1382 m, 1314 w, 1273 w, 1225 w, 1135 m, 1067 w, 1010 w, 959 w, 932 w, 897 w, 835 m, 773 s, 736 m, 546 w.

## X-ray crystallography

A summary of the crystal data and structure refinements for **1–5** is given in Table 1. Single crystal X-ray data for **1–5** were collected on an Enraf-Nonius CAD4 diffractometer with monochromated Mo Kα radiation ($\lambda = 0.71073$ Å) at 123(2) K using phi and/or omega scans. Data were corrected for Lorentz and polarization effects. The structures were solved by direct methods and refined using the full matrix least-squares method of the programs SHELXS-97[34] and SHELXL-97[35] respectively. The program X-Seed[36] was used as an interface to the SHELX programs, and to prepare the figures. In **1**, one of the hydrogen atoms on the water molecule was unable to be located unambiguously and was not included in the model. In

**Table 1** Crystal structure and refinement data for **1–5**

| | 1 | 2 | 3 | 4 | 5 |
|---|---|---|---|---|---|
| Formula | $C_8H_{28}Br_4N_4O_2$ | $C_{12}H_{28}I_{10}N_6$ | $C_{12}H_{44}Cl_6N_6O_4$ | $C_{12}H_{38}Br_4N_6O_2$ | $C_{12}H_{34}I_8N_6$ |
| FW/g $mol^{-1}$ | 531.98 | 1525.40 | 549.23 | 618.12 | 1277.65 |
| Crystal system | Monoclinic | Monoclinic | Triclinic | Orthorhombic | Monoclinic |
| Space group | $C2/c$ | $C2/c$ | $P\bar{1}$ | $Pna2_1$ | $P2_1/c$ |
| $a$/Å | 16.9596(4) | 25.441(5) | 7.2793(2) | 21.5782(1) | 8.1626(2) |
| $b$/Å | 8.8949(2) | 8.0708(16) | 8.0716(3) | 6.2908(5) | 22.7532(5) |
| $c$/Å | 11.6793(3) | 16.777(3) | 11.4099(3) | 17.4204(6) | 8.2545(2) |
| $\alpha$/° | | | 87.859(2) | | |
| $\beta$/° | 94.87(3) | 103.92(3) | 77.590(2) | | 92.970(1) |
| $\gamma$/° | | | 88.234(1) | | |
| Volume/Å$^3$ | 1755.51(7) | 3343.7(12) | 654.10(3) | 2364.7(2) | 1531.01(6) |
| $Z$ | 4 | 4 | 1 | 4 | 2 |
| $\rho_{calcd}$/g $cm^{-3}$ | 2.013 | 3.030 | 1.394 | 1.736 | 2.771 |
| $\mu$ (Mo Kα)/$mm^{-1}$ | 9.172 | 9.280 | 0.685 | 6.824 | 8.114 |
| $\theta$ range/° | 4.08–27.84 | 2.50–28.28 | 3.05–28.29 | 3.01–28.35 | 2.63–28.28 |
| Reflections collected | 10 500 | 15 714 | 7920 | 12 330 | 11 293 |
| Independent reflections | 2071 | 4043 | 3180 | 4796 | 3738 |
| Goodness-of-fit on $F^2$ | 0.98 | 1.019 | 0.973 | 1.018 | 1.03 |
| $R1$[a], $wR2$[b] [$I > 2\sigma(I)$] | 0.0447, 0.1029 | 0.0428, 0.0927 | 0.0472, 0.0873 | 0.0628, 0.1499 | 0.0452, 0.1092 |
| $R1$, $wR2$ all data | 0.0724, 0.1134 | 0.0672, 0.1032 | 0.0855, 0.1005 | 0.0881, 0.1631 | 0.0602, 0.1177 |
| Max. diff. peak and hole, e Å$^{-3}$ | +1.409, −1.496 | +2.086, −2.381 | +0.454, −0.642 | +0.838, −1.349 | +1.652, −2.607 |

[a] $\Sigma||F_o| - |F_c||/\Sigma|F_o|$. [b] $[\Sigma w(F_o^2 - F_c^2)^2/\Sigma\, w(F_o^2)^2]^{1/2}$.

**Table 2** Hydrogen bonds and close contacts in **1**. Esd's are given in parentheses

| D–H···A | *d*(D–H)/Å | *d*(H···A)/Å | *d*(D···A)/Å | ∠(DHA)/° |
|---|---|---|---|---|
| N(1)–H(2)···O(1)W | 0.86(6) | 1.92(6) | 2.757(5) | 167(7) |
| N(1)–H(1)···Br(1) | 0.85(7) | 2.38(7) | 3.187(5) | 157(5) |
| N(2)–H(4)···O(1)W#2 | 0.84(7) | 2.57(6) | 2.954(5) | 109(5) |
| N(2)–H(4)···Br(2)#3 | 0.84(7) | 3.00(7) | 3.746(5) | 150(6) |
| N(2)–H(4)···Br(1)#4 | 0.84(7) | 2.91(8) | 3.386(5) | 118(6) |
| N(2)–H(3)···Br(2) | 0.92(8) | 2.35(8) | 3.269(5) | 178(6) |
| O(1)W–H(1)W···Br(1)#2 | 0.99(1) | 2.42(3) | 3.344(4) | 154(5) |
| C(3)–H(9)···Br(1)#5 | 1.10(6) | 2.62(6) | 3.700(5) | 166(4) |
| N(2)–H(4)···O(1)W#2 | 0.84(7) | 2.57(6) | 2.954(5) | 109(5) |

Symmetry transformations used to generate equivalent atoms: #1 $-x$, $y$, $-z+3/2$; #2 $-x+1/2$, $y+1/2$, $-z+3/2$; #3 $x$, $-y+1$, $z-1/2$; #4 $x$, $y+1$, $z$; #5 $x$, $-y$, $z+1/2$.

all the structures except **2** and **3** the $sp^3$ carbon atoms had hydrogens assigned in calculated positions and refined isotropically with $U(H) = 1.2U_{eq}(C)$. The $sp^3$ carbon atom on the acetonitrile solvent molecule in **2** had hydrogens assigned in calculated positions and refined isotropically with $U(H) = 1.5 U_{eq}(C)$. This was also the case for N(1) and N(4) in **3**. The hydrogen atoms on the amines (N(2) and N(5)) in **4** were unable to be located. All other hydrogen atoms that were located on Fourier difference maps were left unrestrained and refined isotropically. All non-hydrogen atoms were located on Fourier difference maps and refined anisotropically. In all relevant figures dashed lines represent hydrogen bonds. Pertinent geometric parameters are given in the tables and figures, the latter showing 50% probability ellipsoids drawn as ORTEP representations. H-bonding distances discussed within the text are from donor heteroatom (D) to acceptor (A).†

## Results and discussion

The crystallization of the halide adducts was achieved by slow evaporation of aqueous solutions containing one of the macrocycles, **L1** or **L2**, and appropriate quantities of the halic acid. Microanalysis of **1**, **2**, **3**, and **5** provided confirmation that the bulk material was of the same composition as the crystal used in the X-ray structure determination. In the case of **4** this was a minor product with the bulk of the material analysed to be $[H_6\mathbf{L2}Br_6]\cdot 2H_2O$. The IR spectra exhibited a number of absorptions which confirmed the presence of the macrocycles.

### Structure of $[H_4L1(Br)_4]\cdot 2H_2O$ (1)

A list of hydrogen bonds and close contacts for **1** can be found in Table 2. The structure contains a tetraprotonated macrocycle bound to four bromide anions and two water molecules (Fig. 1). The macrocyclic ring lies perpendicular across a plane of symmetry and has all eight ammonium protons directed away from the cavity and participating in H-bonding interactions with bromide and water.

Br(1) is located at the apex of a distorted trigonal pyramid and has contacts with N(1), N(2) (from separate macrocycles) and O(1)W as donors, and there is a long contact with a C–H group that would make the geometry pseudo-tetrahedral if it were to be included as a donor (Fig. 2). The anion lies 0.934(3) Å from the plane of the heteroatom donors and 3.697(2) Å above the least-squares plane of the macrocycle. Br(2) forms a flatter pyramid (0.726(2) Å above the donor plane), having

† CCDC reference numbers 227340–227344. See http://www.rsc.org/suppdata/nj/b4/b401841a/ for crystallographic data in .cif or other electronic format.

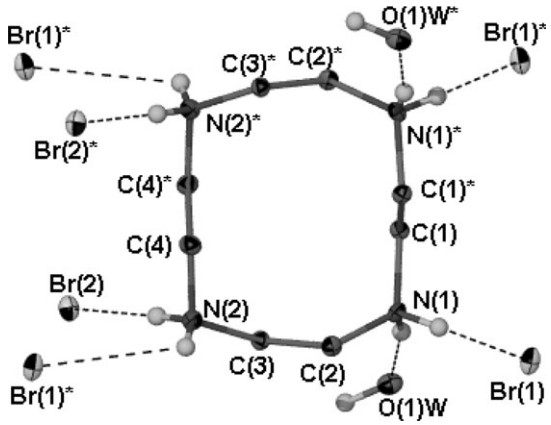


**Fig. 1** ORTEP plot of the hydrogen bonding environment of [12]aneN$_4$ in **1**. C–H hydrogen atoms have been removed for clarity. * represents symmetry-generated atoms.

N(2) and a symmetry-generated pair of water molecules as its base, and lies outside the macrocyclic cavity. The conformation of [12]aneN$_4$ has all of the ammonium protons directed away from the cavity, reflecting the inadequacy of the macrocyclic ring in providing an acceptable conformation capable of docking the large bromide anions. In the analogous chloro adduct of [12]aneN$_4$ described previously[37], the anions are also located on the outside the macrocyclic cavity, indicating that the cavity may be too small to accommodate even chloride. The macrocycle in the chloro adduct was found to adopt the same conformation as that seen in the present structure, enabling it to participate in electrostatic and H-bonding interactions while minimizing ring strain.[37] The bromide anions and water molecules participate in H-bonding interactions that generate 2D sheets more correctly described as 1D chains of composition $Br_x(H_2O)_x$ packed into sheets separated by layers of macrocycles (Fig. 3), the chains being connected only by interactions with the positively charged ammonium groups.

### Structure of $[H_2L1(I_3)_2]\cdot 2I_2\cdot 2CH_3CN$ (2)

Table 3 contains a list of hydrogen bonds and close contacts for **2**. The asymmetric unit consists of one half of a diprotonated macrocycle with one acetonitrile molecule, one $I_3^-$ moiety and one $I_2$ (Fig. 4). The macrocycle lies around a

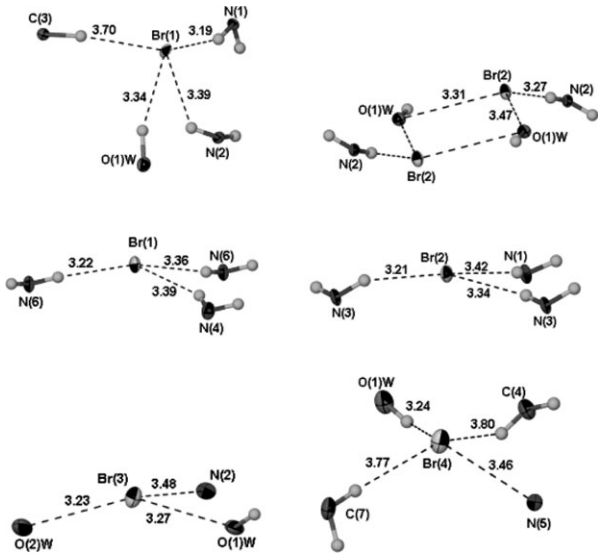


**Fig. 2** ORTEP plots showing the H-bonding interactions of the Br$^-$ anions in **1** (top) and **4** (middle and bottom). Br···N and Br···O interatomic distances are given in Å.

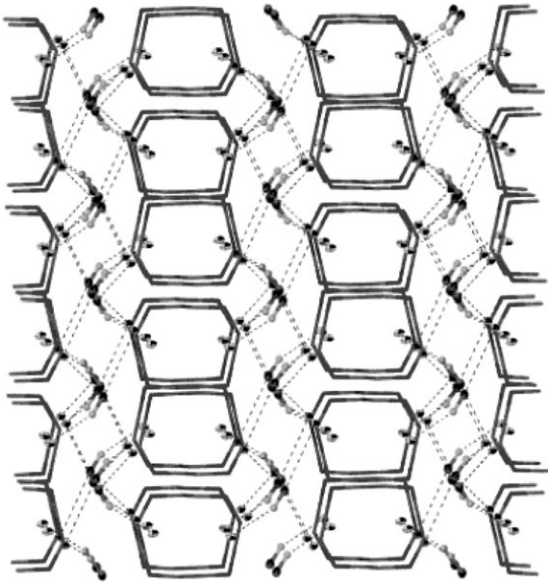

**Fig. 3** Packing of the structure of **1** showing the 2D sheets formed by $Br^-$ and water molecules viewed down the *c* axis. Macrocycles are drawn in stick representation. Dashed lines indicate hydrogen bonds.

twofold axis of symmetry, using one of its ammonium protons to donate a hydrogen bond to the acetonitrile solvent molecule (N(1)–H(2)···N(3): 2.869(9) Å, 150(11)°) which is located away from the cavity in the plane of the ring. An intra-ring interaction between the ammonium and amine nitrogens (N(1)–H(1)···N(2): 2.912(8) Å, 120(6)°) assists in the contraction of the macrocycle in concert with packing effects of the hydrophobic entities.

The iodine atoms assemble into left- and right-handed helices consisting of alternating $I_2$ and $I_3^-$ species (Fig. 5) with the longest intermolecular I···I distance being between I(5) and I(3)* (3.5062(9) Å), which is well below the sum of the van der Waals radii (3.96 Å). Each spiral contains 'grooves', which house macrocycles on two of its four sides, and has acetonitrile molecules occupying its centre. The helices pack with alternating right- and left-handed helices to form infinite channels in which the acetonitrile molecules reside. The protons of the ammonium group N(1) appear to straddle the I(1)···I(2) bond, with the nitrogen being almost equidistant to the two iodines (3.669(6) Å and 3.784(6) Å for I(1) and I(2), respectively). Structures incorporating polyiodide have been previously reported in the literature, including a rotaxane-like assembly,[38] extended 2D networks,[39] extended 3D networks[40] and, very recently, a branched helical arrangement whose backbone is comprised of alternating $I_2$ and $I_3^-$ moieties in a similar manner to that in the present structure.[41] While this structure was created using a helical cation as the template, the helices in **2** have self-assembled without similar coaxing. These examples highlight the versatility of the polyiodide species in adapting to the requirements of a wide range of cationic species.

**Table 3** Hydrogen bonds and close contacts in **2**. Esd's are given in parentheses

| D–H···A | *d*(D–H)/Å | *d*(H···A)/Å | *d*(D···A)/Å | ∠(DHA)/° |
|---|---|---|---|---|
| N(1)–H(1)···N(2)#1 | 0.92(8) | 2.34(8) | 2.912(8) | 120(6) |
| N(1)–H(2)···I(2) | 0.78(11) | 3.37(11) | 3.784(6) | 116(9) |
| N(2)–H(3)···I(3)#1 | 0.95(7) | 3.25(8) | 4.136(6) | 157(5) |
| N(1)–H(2)···N(3) | 0.78(11) | 2.16(11) | 2.869(9) | 150(11) |
| N(1)–H(2)···I(1) | 0.78(11) | 3.31(11) | 3.669(6) | 112(9) |

Symmetry transformation used to generate equivalent atoms: #1 $-x+1, y, -z+3/2$.

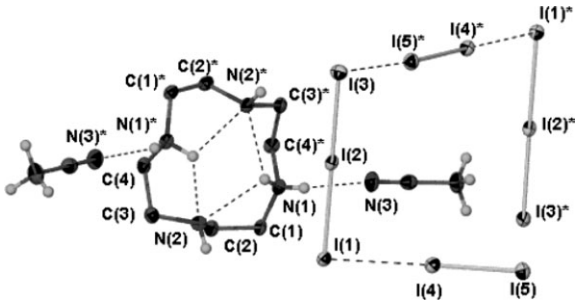


**Fig. 4** ORTEP plot of the expanded asymmetric unit of **2**. Selected interatomic distances: I(1)···I(2) 3.012(1), I(2)···I(3) 2.831(1), I(4)···I(5) 2.7516(8), I(1)···I(4) 3.3090(8), I(3)···I(5)* 3.5062(9). Macrocyclic C–H hydrogen atoms have been removed for clarity. Dashed lines represent H-bonds and close contacts. * indicates symmetry generated atoms.

### Structure of $[H_6L2(Cl)_6]\cdot 4H_2O$ (3)

This structure is the only one in the series in which **L2** is fully protonated and thus contains a full compliment of ammonium groups (Figs. 6 and 7). Table 4 contains a list of hydrogen bonds and close contacts.

Fig. 6 shows the hydrogen bonding environment around the macrocycle, which utilizes all 12 ammonium protons in interactions with either water or the chloride anions. Owing to the greater charge of the protonated macrocycle (6+), the macrocyclic cavity is much larger than that found in **4** and **5** (150 $Å^2$ *cf.* 106 $Å^2$ for both **4** and **5**. Interestingly, the conformation adopted by the macrocycle in **3** is also the most distorted from a 'regular' conformation (Fig. 6) (which would have equal N···N distances for N(1)···N(1)*, N(2)···N(2)* and N(3)···N(3)*) of the three [18]ane$N_6$ presented. In rationalizing this behaviour, it should be noted that once the macrocycle is in contact with two chloride ions (Cl(1) and Cl(1)*) through four ammonium groups, there is still a charge of 4+ to be compensated for. As the macrocyclic cavity is not sufficiently large to hold two $Cl^-$ anions on each side, it is elongated along the axis of the two remaining ammonium groups that are each pointing outwards to interact with water and chloride anions, that form part of a negatively charged chain comprised of $Cl^-$ and water in a 1 : 1 ratio. The extended structure of **3** is best described as 2D sheets that are connected by a single C–H···Cl interaction (3.419(2) Å, 137(2)°, Fig. 7).

There are three crystallographically unique chlorides in the structure (Fig. 8). Cl(1) sits 2.024(2) Å above from the mean plane of the macrocyclic cavity, forming the apex of a trigonal pyramid, the base of which is made up of three close contacts with two ammonium donors and a C–H from the same macrocycle. The N–H···Cl(1) contacts are quite short: 3.095(2) Å from N(3) and 3.203(5) Å from N(2), and the C–H···Cl(1) interaction is close to linear (C(5)–H(15)···Cl(1) 3.588(3) Å, 165(2)°). A recent statistical survey of the CSD has shown unequivocally that a short C–H···$Cl^-$ represents a real interaction with a strong angular dependence.[42] This

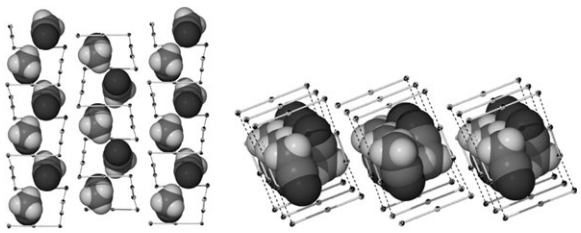

**Fig. 5** Packing diagram of the iodine moieties and acetonitrile molecules in **2** viewed along the *a* axis (left) and the *b* axis (right) showing the alternating left- and right- handed helices (middle helix is left-handed in both figures). Iodine atoms are shown in ORTEP representation and acetonitrile in van der Waals representation.

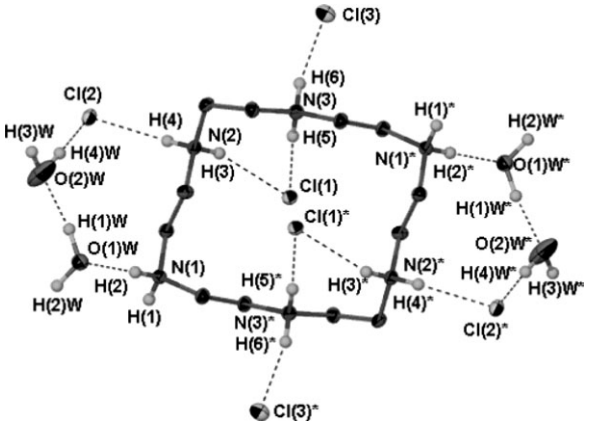


**Fig. 6** ORTEP plot showing the H-bonding environment around the macrocycle in **3**. C–H hydrogen atoms are removed for clarity. Dashed lines represent H-bonds. * indicates symmetry generated atoms.

C–H···Cl(1) interaction is a clear example of an ideally placed C–H group contributing to overall adduct stability by occupying a site which enables interaction with the halide. There is another close C–H···Cl contact in **3** between Cl(3) and a carbon atom from a neighbouring macrocycle (C(2)–H(10)···Cl(3) 3.415(5) Å, 138°), which makes this chloride different to the others in that the donor groups adopt a distorted tetrahedral geometry around the chloride. The trigonal pyramidal H-bonding motif formed around Cl(1) and Cl(2) is more common and has been previously found to be adopted by chloride anions in the less co-ordinatively-restrictive environment of non-cyclic polyamines.[32] In our work, this was also the most commonly observed H-bonding cluster in the five chloride structures. Given the recurrence of this motif we have found it useful to characterize the trigonal pyramid by the distance that the chloride lies from the plane defined by the three H-bond donors comprising the base of the trigonal pyramid, and the D···A···D chelate angles, which provide a measure of the departure from a regular trigonal pyramid. Deviations from the planes defined by the donors to Cl(1) and Cl(2) in **3**, were calculated as 1.842(4) Å and 1.476(3) Å, respectively. For Cl(3), the deviation from the N–N–O plane is 1.566(3) Å, however it is 0.200(3) Å from the N–N–C plane. The chelate bite angles of the macrocycle are 59° for the two adjacent ammonium groups and 85° for N(2)–Cl(1)–C(5).

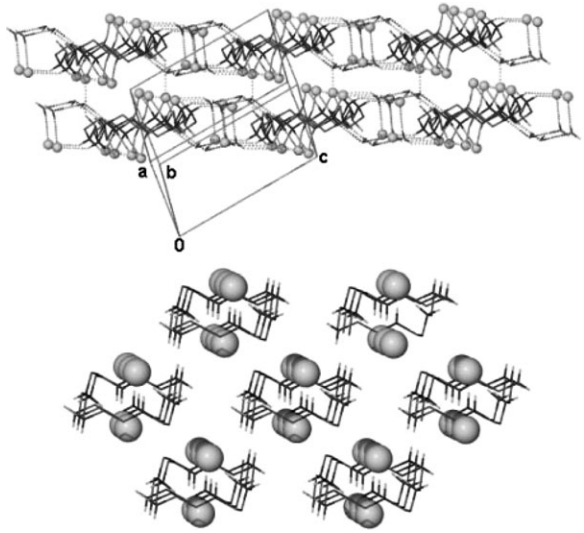


**Fig. 7** Packed view of the hydrogen bonding network in **3** viewed parallel to the 2D sheets (ORTEP representation, top) and packed view of the **L2**$Cl_2$ units with water and chlorides exterior to the cavity removed with $Cl^-$ shown as 1/2 van der Waals spheres with the macrocycle in stick representation viewed along the *c* axis (bottom).

**Table 4** Hydrogen bonds and close contacts in **3**. Esd's are given in parentheses

| D–H···A | *d*(D–H)/Å | *d*(H···A)/Å | *d*(D···A)/Å | ∠(DHA)/° |
|---|---|---|---|---|
| N(3)–H(6)···Cl(3) | 0.87(3) | 2.23(3) | 3.075(2) | 167(2) |
| N(1)–H(2)···O(1)W | 0.88(3) | 1.88(3) | 2.757(3) | 174(2) |
| N(1)–H(1)···Cl(3)#2* | 0.89(3) | 2.19(3) | 3.048(2) | 163(2) |
| N(3)–H(5)···Cl(1) | 0.94(3) | 2.15(3) | 3.095(2) | 178(2) |
| N(2)–H(3)···Cl(1) | 0.97(3) | 2.36(3) | 3.203(2) | 146(2) |
| N(2)–H(3)···O(1)W#3 | 0.97(3) | 2.54(3) | 3.131(3) | 119(2) |
| O(1)W–H(2)W···Cl(2)#4 | 0.78(4) | 2.37(4) | 3.143(2) | 167(3) |
| O(1)W–H(1)W···O(2)W | 0.85(3) | 1.86(3) | 2.712(3) | 174(3) |
| O(2)W–H(4)W···Cl(2) | 0.77(5) | 2.37(5) | 3.138(3) | 171(4) |
| O(2)W–H(3)W···O(2)W#5 | 0.72(5) | 2.63(4) | 3.102(7) | 125(4) |
| O(2)W–H(3)W...Cl(3)#6 | 0.72(5) | 2.66(4) | 3.241(3) | 140(4) |
| N(2)–H(4)···Cl(2) | 0.93(3) | 2.23(3) | 3.071(2) | 149(2) |
| N(2)–H(4)···Cl(2)#7 | 0.93(3) | 2.81(3) | 3.299(2) | 114(2) |
| C(5)–H(15)···Cl(1)#1 | 0.97(3) | 2.64(3) | 3.588(3) | 165(2) |
| C(2)–H(10)···Cl(3)#8 | 1.02(3) | 2.60(2) | 3.419(2) | 137(2) |

Symmetry transformations used to generate equivalent atoms: #1 $-x+1, -y, -z+2$; #2 $x-1, y+1, z$; #3 $x, y-1, z$; #4 $-x+1, -y+1, -z+1$; #5 $-x+2, -y+1, -z+1$; #6 $-x+2, -y, -z+1$; #7 $-x+1, -y, -z+1$; #8 $x, y+1, z$.

### Structure of $[H_4L2(Br)_4]\cdot 2H_2O$ (4)

A list of all H-bonds and close contacts for **4** is given in Table 5. The crystal structure of **4** contains a tetraprotonated hexaazamacrocycle H-bonding to four bromide anions and two water molecules (Fig. 9). As with the macrocyclic amines in **2**, the protons on the two amine nitrogens in **4** could not be located on Fourier difference maps and were not modelled, however the proximity of a bromide (Br(3)···N(2), 3.48 Å Br(4)*···N(5), 3.46 Å) to each one suggests that this hydrogen atom points in the general direction of the anion with their lone pairs oriented towards the centre of the macrocycle. This is corroborated by two intra-ring N–H···N interactions (N(3)–H(3)···N(2) 2.798(12) Å, 105° N(6)–H(8)···N(5) 2.793(12) Å, 104°) that assist in the elongation of the macrocycle along the axis defined by the two amines. The two bromides that lie above and below the ring (Br(1) and Br(2)) are in a trigonal pyramidal environment similar to that found for chlorides in **3**, each being chelated by two ammonium groups from their host macrocycle and one from a neighbouring macrocycle (Fig. 2). These two anions lie 1.954(3) Å and 1.960(3) Å from the mean plane of the macrocyclic cavity, in surprising contrast to the larger distance of 2.024(2) Å found for the smaller chloride anion in **3**, which also had a larger and more electropositive macrocyclic cavity to occupy! The co-ordination pyramids (Fig. 3) formed in this case are considerably flatter than those for the chlorides, with deviations from the planes of their three

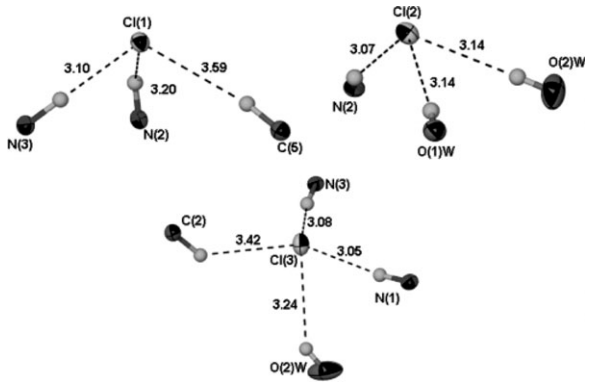


**Fig. 8** ORTEP plots showing the H-bonding interactions of the $Cl^-$ anions in **3**. D···$Cl^-$ distances are given in Å.

**Table 5** Hydrogen bonds and close contacts in **4**. Esd's are given in parentheses except for fixed and riding H

| D–H···A | *d*(D–H)/Å | *d*(H···A)/Å | *d*(D···A)/Å | ∠(DHA)/° |
|---|---|---|---|---|
| N(1)–H(1)···O(1)W | 0.92 | 1.87 | 2.71(1) | 150.8 |
| N(1)–H(2)···Br(2) | 0.92 | 2.61 | 3.416(8) | 146 |
| N(1)–H(2)···Br(1) | 0.92 | 2.88 | 3.397(8) | 116.6 |
| N(3)–H(4)···Br(2)#1 | 0.92 | 2.41 | 3.213(7) | 146.4 |
| N(3)–H(4)···Br(1) | 0.92 | 2.87 | 3.363(8) | 115 |
| N(3)–H(3)···Br(2) | 0.92 | 2.49 | 3.343(8) | 153.8 |
| N(4)–H(6)···Br(1) | 0.92 | 2.57 | 3.394(8) | 148.8 |
| N(4)–H(6)···Br(2) | 0.92 | 2.86 | 3.327(8) | 112.9 |
| N(4)–H(5)···O(2)W | 0.92 | 1.89 | 2.741(11) | 152.1 |
| N(6)–H(7)···Br(1)#2 | 0.92 | 2.4 | 3.222(8) | 149.3 |
| N(6)–H(7)···Br(2) | 0.92 | 2.95 | 3.412(9) | 112.7 |
| N(6)–H(8)···Br(1) | 0.92 | 2.5 | 3.363(8) | 155.6 |
| O(1)W–H(2)W···Br(4) | 1.00(1) | 2.32(7) | 3.239(7) | 153(12) |
| N(3)–H(3)···N(2) | 0.92 | 2.41 | 2.798(12) | 105.6 |
| N(6)–H(8)···N(5) | 0.92 | 2.42 | 2.793(12) | 104.1 |

Symmetry transformations used to generate equivalent atoms: #1 $x$, $y+1$, $z$; #2 $x$, $y-1$, $z$.

donors being 0.629(7) Å and 0.626(7) Å for Br(1) and Br(2), respectively. The arrangements of atoms around the two remaining bromide anions, Br(3) and Br(4), are also relatively flat and close to trigonal pyramidal. In this case, however, the donors comprise two water molecules and a macrocyclic amine for each, inferred from the nearness of the contacts (Table 5). Br(3) is locked between water molecules, O(1)W* and O(2)W* (3.270(7) Å and 3.232(9) Å, respectively), which themselves are also interacting with the macrocyclic ammonium protons, and a macrocyclic ammonium group, N(2) (3.478(8) Å). The deviation from the plane of its donors is calculated as 0.655(5) Å. The next two closest contacts are with two carbon atoms each at least 3.84 Å away. Br(4) accepts H-bonds from O(1)W and O(2)W* (3.2397(7) Å and 3.281(10) Å, respectively) and from N(5)* (3.464(8) Å). It lies almost precisely within the plane of the three donors (deviation from the donor plane of 0.188(5) Å) and has a possible weak interaction in an almost linear C–H···Br contact (3.769(11) Å, 171°).

Fig. 10 illustrates undulating 2D sheets formed by the bromides (Br(3) and Br(4)) and the water molecules between which lie layers of macrocycles, each chelating the two remaining bromides through ammonium groups. Removal of these interstitial $Br^-$ and water molecules reveals a 1D chain com-

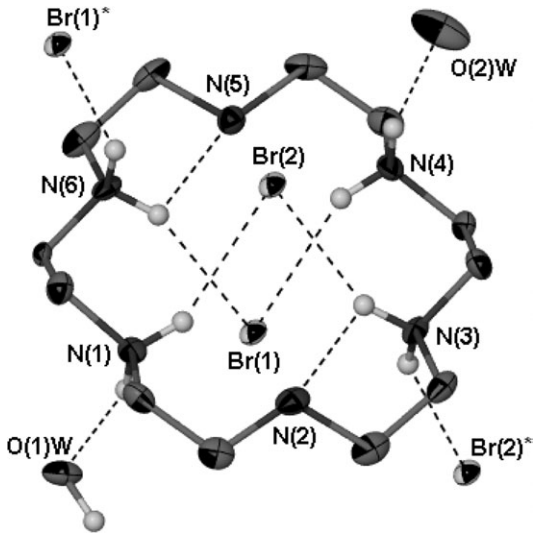


**Fig. 9** ORTEP plot of the hydrogen bonding environment of the macrocycle in **4**. C–H hydrogen atoms have been removed for clarity. Dashed lines represent close contacts and hydrogen bonds. * indicates symmetry generated atoms.

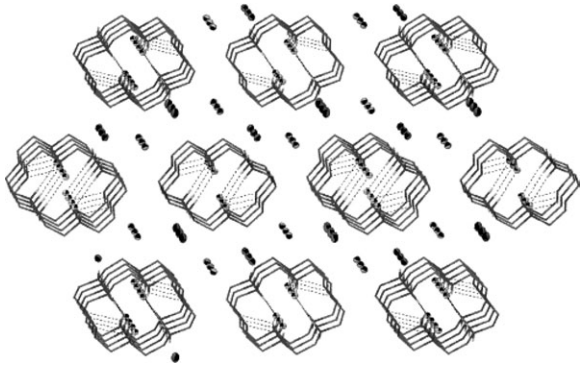

**Fig. 10** Packing of the anions, water and macrocycles in **4** viewed along the *b* axis showing the horizontal sheets of bromide and water molecules. Bromide (yellow) and oxygen (red) atoms are shown in ORTEP representation.

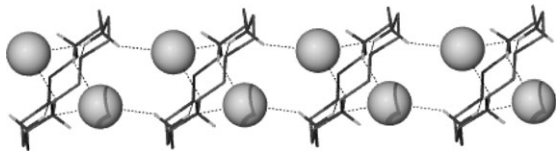

**Fig. 11** 1D chains formed by the macrocycles and two of the four crystallographically unique bromide anions in **4** (viewed along the *a* axis). Dashed lines represent hydrogen bonds.

prised of parallel macrocycles sandwiching their chelated bromide anions (Fig. 11). In contrast to **3**, the macrocycle has all nitrogen atoms oriented towards its centre (Fig. 9). The chelate bite angle for the macrocycle is 83°, similar to that found for the N–Cl–C angle in **3**.

### Structure of $[H_4L2(I)_2(I_3)_2]$ (5)

Hydrogen bonding and close contact details for **5** can be found in Table 6. The structure of **5** consists of a tetraprotonated macrocycle lying around a crystallographic inversion centre with the charge being balanced by two $I^-$ and two $I_3^-$ anions (Fig. 12). There are no solvent molecules in the lattice and in contrast to **2** and **4**, proton H(5) on the amine nitrogen (N(3)) was located unambiguously in Fourier difference maps, its position also being corroborated by the presence of a hydrogen bond to the N(3) lone pair from an adjacent ammonium group (N(1)–H(2)···N(3)* 2.828(8) Å, 107°). This interaction, as in the other structures, contributes to the elongation of the macrocycle along the axis defined by the amines, N(3) and N(3)*.

**Table 6** Hydrogen bonds and close contacts in **5**. Esd's are given in parentheses except for fixed and riding H

| D–H···A | *d*(D–H)/Å | *d*(H···A)/Å | *d*(D···A)/Å | ∠(DHA)/° |
|---|---|---|---|---|
| N(1)–H(1)···I(4)#2 | 0.92 | 2.85 | 3.591(6) | 138.7 |
| N(1)–H(1)···I(1)#1 | 0.92 | 3.11 | 3.595(5) | 114.5 |
| N(1)–H(2)···I(1) | 0.92 | 2.89 | 3.669(6) | 143.2 |
| N(2)–H(3)···I(1)#1 | 0.92 | 2.78 | 3.605(6) | 150.1 |
| N(2)–H(4)···I(4)#3 | 0.92 | 2.91 | 3.598(6) | 132.5 |
| N(2)–H(4)···I(1) | 0.92 | 3.04 | 3.581(6) | 119.2 |
| N(3)–H(5)···I(1)#4 | 1.00(1) | 3.17(7) | 3.868(6) | 128(6) |
| N(1)–H(2)···N(3)#1 | 0.92 | 2.43 | 2.828(8) | 106.5 |
| N(2)–H(4)···I(1) | 0.92 | 3.04 | 3.581(6) | 119.2 |
| N(1)–H(1)···I(1)#1 | 0.92 | 3.11 | 3.595(5) | 114.5 |
| N(2)–H(3)···I(1)#1 | 0.92 | 2.78 | 3.605(6) | 150.1 |

Symmetry transformations used to generate equivalent atoms: #1 $-x+2$, $-y+1$, $-z+2$; #2 $x$, $-y+1/2$, $z+1/2$; #3 $x$, $-y+1/2$, $z-1/2$; #4 $x-1$, $y$, $z$.

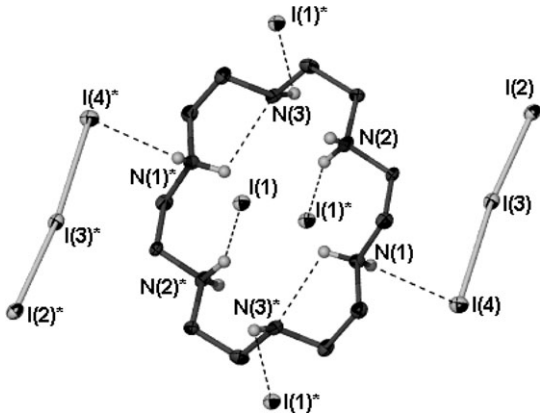


**Fig. 12** ORTEP view of the hydrogen bonding network around the macrocycle in **5**. C–H hydrogen atoms have been removed for clarity. * indicates symmetry generated atoms.

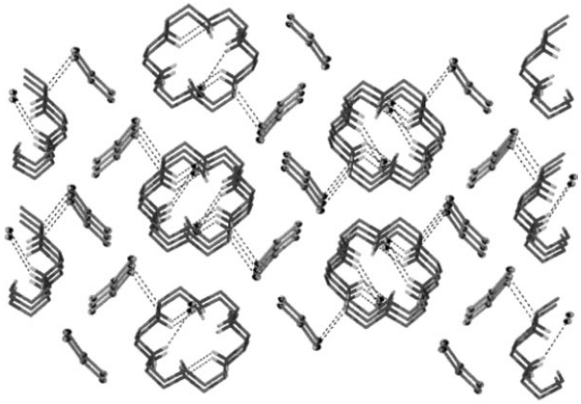

**Fig. 13** Packing diagram of the macrocycle (stick representation) and iodide moieties (ORTEP representation) in **5** viewed along the *a* axis.

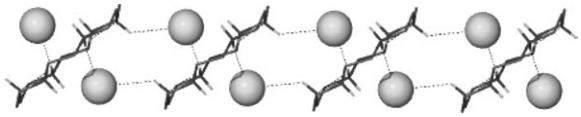

**Fig. 14** 1D chains formed by $I^-$ and the macrocycles in **5**. Iodides are drawn as $\frac{1}{2}$ van der Waals spheres.

The large, linear $I_3^-$ anions lie outside the macrocyclic cavity, forming undulating sheets much like those formed by bromide and water in **4** (Fig. 13), with sheets of $[H_4\mathbf{L2}(I)_2]^{2+}$ cations separating the layers. Each $I_3^-$ is participating in a total of two hydrogen bonding interactions through I(4) with two macrocyclic ammonium protons (N(1)–H(1)···I(4)* 3.591(6) Å, 138.7° and N(2)*–H(4)*···I(4)* 3.598(6) Å, 132.5°). There is a significant difference between distances from the central iodine atom (I(3)) of the anion to those on the ends (I(2)···I(3) 2.8034(9) Å, I(3)···I(4) 3.158(1) Å, reflecting the polarizing effect of the two H-bonds to I(4). This asymmetry is less pronounced in the $I_3^-$ anion in **2** (I···I distances of 3.012(1) Å (I(1)···I(2)) and 2.831(1) Å (I(2)···I(3)) which is participating in longer and less directional H-bonds, and with only one donor. The $I^-$ anion is participating in H-bonding with three macrocyclic ammonium groups and lies 2.351(1) Å above the mean plane of the macrocyclic cavity, an expected increase on the analogous situation for the chelated bromide in **3**. In examining the 1D chains formed by the macrocycles and anions in **4** and **5** (see Figs. 11 and 14) it is interesting to note that the bromides each utilize three N–H···X interactions in their formation whereas the iodides only use two. As with the other halides, the co-ordinated iodine atoms are at the apex of a trigonal pyramid if we take I(4) to have I(3) as its 'donor'. Deviations from the donor planes are 2.367(1) for I(1) and 1.210(3) for I(4). The chelate bite angle of the macrocycle is 75°, slightly smaller than that for bromide in **4** as one would expect due to the longer interactions. The tetraprotonated macrocycle has a similar conformation to that seen in **4** with all nitrogen atoms directed towards the cavity centre and an elongation along one of the N···N* axes.

## Conclusion

We have described the X-ray crystal structures of a series of azamacrocycle–halide adducts, and the factors contributing to the formation of various H-bonding constructs observed therein. The cavity of protonated [12]aneN$_4$ is not sufficiently large to bind $Cl^-$, $Br^-$ or $I^-$ within the macrocyclic cavity and, as a consequence, the anions are located on the exterior of the macrocycle, and the conformation of the macrocycle is adjusted to facilitate crystallization through H-bonding interactions with the amine and ammonium groups. The larger [18]aneN$_6$ macrocycle, on the other hand, is able to participate in hydrogen bonding interactions with anions both on the inside and the outside of the cavity. In addition to assisting crystallization in similar ways to [12]aneN$_4$, [18]aneN$_6$ is able to bind two halide anions within the macrocycle cavity and, in the case of chloride, exclusively through interactions with N–H or $NH_2^+$ groups on a single macrocycle. Although this appears to contradict the findings of the solution studies,[31] where one halide binds to the macrocycle, we note that our products have been isolated at low pH and from solutions containing higher halide concentrations than used to determine binding constants.

Nevertheless, the structural motifs that we have elucidated do highlight a number of features that are likely to make important contributions to the binding of these halides in solution.[31] In this context, both $Br^-$ and $Cl^-$ have a tendency to form trigonal pyramidal arrays with three H-bond donors, with $Cl^-$ invariably sitting further from the plane of the donors. This particular structural feature was highlighted by Ilioudis *et al.*[32] where trigonal pyramidal constructs were formed by chloride (and to a lesser extent, bromide, which had a tendency towards square pyramidal geometries) anions when co-ordinated to a series of linear polyammonium cations. As in our study, these ligands adopt flexible co-ordination geometries that respond to anion size. Moreover, as the size of the anion increases, interactions involving neighbouring macrocycles become more important as it becomes more difficult to fit the larger anions close to or within the cavity. As indicated previously,[32] in contrast to existing studies in which pre-organized hosts largely determine the halide coordination environment, the use of flexible open chain and branched protonated polyamine ligands and also flexible protonated mono-macrocyclic ligands, [18]aneN$_6$ more so than [12]aneN$_4$, is allowing the elucidation of the preferred halide coordination modes in less constrained environments. Ongoing studies are focusing on adducts formed by protonated forms of [12]aneN$_4$, [15]aneN$_5$ and [18]aneN$_6$ and a wider variety of anions.

## Acknowledgements

This research was supported by the Australian Research Council. ACW gratefully acknowledges the receipt of a Monash University Teaching Fellowship and a Monash Departmental Scholarship.

## References

1 P. D. Beer and P. A. Gale, *Agnew. Chem., Int. Ed.*, 2001, **40**, 486.
2 *Supramolecular Chemistry of Anions*, ed. A. Bianci, K. Bowman-James and E. Garcia-España, Wiley-VCH, New York, 1997.
3 C. H. Park and H. E. Simmons, *J. Am. Chem. Soc.*, 1968, **90**, 2431.

4 R. A. Bell, G. G. Christoph, F. R. Fronczek and R. E. Marsh, *Science*, 1975, **190**, 151.
5 B. Metz, J. M. Rosalky and R. Weiss, *J. Chem. Soc., Chem. Commun*., 1976, 533.
6 J.-M. Lehn, *Acc. Chem. Res*., 1978, **11**, 49.
7 F. P. Schmidtchen and G. Müller, *J. Chem. Soc., Chem. Commun*., 1984, 1115.
8 B. Deitrich, J. Guilhem, J.-M. Lehn, C. Pascard and E Sonveaux, *Helv. Chim. Acta*, 1984, **67**, 91.
9 B. Deitrich, J.-M. Lehn, J. Guilhem and C. Pascard, *Tetrahedron Lett*., 1989, **30**, 4125.
10 J. L. Sessler, M. J. Cyr, V. Lynch, E. McGhee and J. A. Ibers, *J. Am. Chem. Soc*., 1990, **112**, 2810.
11 J. L. Sessler, T. Morishima and V. Lynch, *Agnew. Chem., Int. Ed. Engl*., 1991, **30**, 977.
12 M. Shionoya, H. Furuta, V. Lynch, A. Harriman and J. L. Sessler, *J. Am. Chem. Soc*, 1992, **114**, 5714.
13 J. Sessler, D. An, W.-S. Cho and V. Lynch, *Agnew. Chem., Int. Ed*., 2003, **42**, 2278.
14 G. Cafeo, F. Kohnke, G. L. La Torre, A. J. P. White and D. J. Williams, *Chem. Commun*., 2000, 1207.
15 D-W. Yoon, H. Hwang and C–H. Lee, *Agnew. Chem., Int. Ed*., 2002, **41**, 1757.
16 B. Turner, A. Shterenberg, M. Kapon, K. Suwinska and Y. Eichen, *Chem. Commun*., 2001, 13.
17 P. A. Gale, S. Camiolo, C. P. Chapman, M. E. Light and M. B. Hursthouse, *Tetrahedron Lett*., 2001, **42**, 5095.
18 S. O. Kang, J. M. Linares, D. Powell, D. VanderVelde and K. Bowman-James, *J. Am. Chem. Soc*., 2003, **125**, 10 152.
19 M. A. Hossain, S. O. Kang, D. Powell and K. Bowman-James, *Inorg. Chem*., 2003, **42**, 1397.
20 S. Kubic and R. Goddard, *Proc. Natl. Acad. Sci. USA*, 2002, **99**, 5127.
21 A. Szumna and J. Jurczak, *Eur. J. Org. Chem*., 2001, 4031.
22 Y-J. Cheng, Z-M. Wang, C-S. Liao and C–H. Yan, *New J. Chem*., 2002, **26**, 1360.
23 Y. Yuan, G. Gao, Z-L. Jiang, J-S. You, Z-Y. Zhou, D-Q. Yuan and R-G. Xie, *Tetrahedron*, 2002, **58**, 8993.
24 X. Wang and J. J. Vittal, *Inorg. Chem*., 2003, **42**, 5135.
25 M. Iwaoka, H. Komatsu and S. Tomoda, *J. Organomet. Chem*., 2000, **611**, 164.
26 V. Amendola, E. Bastianello, L. Fabbrizzi, C. Mangano, P. Pallavicini, A. Perotti, A. M. Lanfredi and F. Ugozzoli, *Agnew. Chem., Int. Ed*., 2000, **39**, 2917.
27 M. Mascal, *J. Chem. Soc., Perkin Trans. 2*, 1997, 1999.
28 A. Barnes, Z. Latajka and M. Biczysko, *J. Mol. Struct*., 2002, **614**, 11.
29 A. Chaumont, E. Engler and G. Wipff, *Chem. Eur. J*., 2003, **9**, 635.
30 C. Garau, D. Quiñonero, A. Frontera, A. Costa, P. Ballester and P. M. Deyà, *Chem. Phys. Lett*., 2003, **370**, 7.
31 J. Cullinane, R. I. Gelb, T. N. Margulis and L. J. Zompa, *J. Am. Chem. Soc*., 1982, **104**, 3048; R. M. Izatt, K. Pawlak and J. S. Bradshaw, *Chem. Rev*., 1991, **91**, 1721.
32 C. A. Ilioudis, K. S. B. Hancock, D. G. Georganopoulou and J. W. Steed, *New J. Chem*., 2000, **24**, 787.
33 A. C. Warden, M. Warren, M. T. W. Hearn, and L. Spiccia, *Inorg. Chem*., submitted.
34 G. M. Sheldrick, *SHELXS-97*, University of Göttingen, Germany, 1997.
35 G. M. Sheldrick, *SHELXL-97*, University of Göttingen, Germany, 1997.
36 L. J. Barbour, X.-Seed-A software tool for supramolecular crytallography, *J. Supramol. Chem*., 2001, **1**, 189.
37 J. H. Reibenspies and O. P. Anderson, *Acta Crystallogr., Sect. C: Cryst. Struct. Commun*., 1990, **46**, 163.
38 Z. Wang, Y. Cheng, C. Liao and C. Yan, *Cryst. Eng. Commun*., 2001, **50**, 1.
39 C. Horn, M. Scudder and I. Dance, *Cryst. Eng. Commun*., 2001, **2**, 1.
40 A. J. Blake, R. O. Gould, W-S. Li, V. Lippolis, S. Parsons, C. Radek and M. Schröder, *Inorg. Chem*., 1998, **37**, 5070.
41 C. J. Horn, A. J. Blake, N. R. Champness, A. Garau, V. Lippolis, C. Wilson and M. Schröder, *Chem. Commun*., 2003, 312.
42 C. B. Aakeröy, T. A. Evans, K. R. Sneddon and I. Pálinkó, *New J. Chem*., 1999, 145.